Influence of vacuum chamber port terminations on beam coupling impedances

Thomas Flisgen*
Ferdinand-Braun-Institut gGmbH, Leibniz-Institut für Höchstfrequenztechnik, Gustav-Kirchhoff-Straße 4, 12489 Berlin, Germany

Shahnam Gorgi Zadeh
European Organization for Nuclear Research (CERN), Meyrin 1217, Switzerland

Erion Gjonaj
Institute for Accelerator Science and Electromagnetic Fields (TEMF), Technische Universität Darmstadt, Schloßgartenstraße 8, 64289 Darmstadt, Germany

(Received 3 June 2022; accepted 17 November 2022; published 6 January 2023)

Vacuum chambers of particle accelerators are typically equipped with radio-frequency couplers. The couplers are employed to excite modes for particle acceleration, to extract the energy of higher-order modes, or for diagnostic purposes. From a network theory perspective, these couplers represent terminal ports by which means the structure can exchange energy with its exterior. Usually, these ports are terminated with fixed impedances corresponding to the characteristic impedances of the coaxial lines attached to them. In this paper, we investigate the influence of the termination conditions of vacuum chambers on beam coupling impedances. For this purpose, we introduce a novel approach that allows us to determine beam coupling impedances for arbitrary port terminations. A full-wave Maxwell solver is employed to determine a generalized scattering matrix of the vacuum chamber and its couplers terminated with prespecified reference impedances. Often, these impedances are chosen to be the characteristic line impedances of the waveguides so that coupler ports are free of reflection. Using the generalized scattering matrix, the beam coupling impedances can be readily determined by means of a computationally inexpensive postprocessing step that takes into account arbitrary impedance loads at the coupler ports. Thus, the influence of various port terminations on the beam coupling impedances can be conveniently examined. This is relevant to improve older structures that were designed when no sophisticated design tools were available or to improve the operation of existing structures for a purpose they were initially not designed for. Using the proposed approach, we investigate the 33-cell 200 MHz traveling-wave accelerating structures of the SPS at CERN. It is shown that port termination conditions do have an important influence on the beam coupling impedance and, therefore, must be taken into account in beam stability considerations.

DOI: 10.1103/PhysRevAccelBeams.26.014601

I. INTRODUCTION

Charged-particle beams traversing vacuum chambers of particle accelerators excite electromagnetic wakefields [1–5]. The interaction of these wakefields with the particle beam may lead to instabilities, thus, limiting the maximal achievable beam current. Furthermore, wakefields can be responsible for other unwanted effects such as deterioration of beam quality and/or excessive heat load on the lossy walls of the vacuum chamber.

The wakefield interaction is typically characterized in the time domain by so-called wake potentials and in the frequency domain by the corresponding beam coupling impedances. The measurement, the analytical calculation as well as the numerical computation of beam coupling impedances have been addressed by many authors in the past (see e.g., [6–16] and references therein).

The ever-increasing demand for high beam currents with short pulses requires the accurate estimation of beam coupling impedances in a broad frequency band as discussed, e.g., in [17]. Consequently, guidelines to ensure low beam coupling impedances are already required in the early design stages. For impedance studies, a number of

*thomas.flisgen@fbh-berlin.de

numerical codes such as ECHO [18], PBCI [19], GdfidL [20], ACE3P [21], and CST Studio Suite® [22] are available in addition to analytical methods [3,14–16]. These codes are able to compute with great accuracy impedance contributions arising from surface effects such as wall resistance and from geometrical effects such as changes in the cross section of the vacuum chamber.

Usually, the vacuum chambers are equipped with radio-frequency (rf) couplers. For instance, such couplers are employed to excite modes for particle acceleration or are used for diagnostic purposes. Methods to design rf couplers for vacuum chambers are well developed and have been used for decades. The design methods and the underlying models are predominantly based on the analysis of the electromagnetic field distributions resulting from the excitation of waveguides with probes and loops [23,24]. Higher-order mode (HOM) couplers are another special type of couplers which are used to extract the energy of unwanted modes within the structure. The HOM couplers are designed such that dangerous modes in the vacuum chamber are damped by (typically prespecified) resistive termination loads, whereas the fundamental mode should remain unaffected. Typical design methods [25–29] for HOM couplers are based on 3D electromagnetic field simulations accompanied by equivalent circuit diagrams including lumped network elements and transmission lines. Nowadays, often existing coupler designs are chosen as a starting point and are modified to satisfy the required figures of merit.

Despite the well-established knowledge that beam coupling impedances can be changed with comparably less effort by modifying coupler termination impedances, studies directly related to the influence of these terminations on beam coupling impedances are scarce. As an exception to the rule, in [30,31] it was proposed to reduce the beam coupling impedance of the CERN Super Proton Synchrotron (SPS) at 630 MHz by reducing the termination impedances of the traveling-wave (TW) structures from 50 Ω to approximately 23 Ω. This was an extremely important observation since the high-order modes around 630 MHz have been identified as one of the main sources of longitudinal multibunch instabilities at the SPS [30–32].

The relative lack of attention in the literature on the influence of port terminations on beam coupling impedances is probably a matter of methodology. Typically, the coupler design process consists of the following sequence of steps. In the first step, an overall beam impedance threshold is determined by beam dynamics simulations and stability considerations. Next, the investigation of cavities and other parts of the vacuum chamber gives coupling constants for relevant (higher-order) modes in these structures. The beam impedance threshold provides the upper bound for the shunt impedances of these modes. Subsequently, couplers terminated with prespecified termination impedances are designed such that the constraints on the quality factors are met. Finally, various iterations of the described approach may be required to converge to a satisfying coupler design. In this procedure, however, termination impedances are considered as fixed parameters and are, therefore, not a degree of freedom in the optimization process.

Another reason that discourages a thorough investigation of the impact of coupler terminations on the beam coupling impedance is that wakefield or impedance simulations with varying port terminations are numerically extremely time consuming. For every set of port terminations at the couplers, generally, a full-scale simulation of the complete chamber structure—typically in 3D—is required.

The aim of this paper is to introduce an approach that readily allows for determining the beam coupling impedance for various termination impedances at the coupler ports. The scheme is based on the idea of the generalized scattering matrix introduced in [33]. In the generalized scattering matrix formulation, the charged particle beam is considered as an independent excitation port in the N-port network model representing the loaded vacuum chamber. This frequency-dependent generalized scattering matrix needs to be determined only once for the given chamber geometry with attached waveguide ports, terminated with prespecified impedances (typically the characteristic impedances of the waveguides). This requires the numerical solution of Maxwell's equations which is typically conducted using finite-element approaches or the finite-integration technique. Once the generalized scattering matrix is known in the frequency interval of interest, the beam coupling impedance resulting from various termination conditions at the coupler ports can be easily determined using the approach described in this paper. We believe this is the first method that allows for conveniently computing beam coupling impedances for different termination impedances of the radio-frequency couplers. The method is particularly suitable to improve the operation of existing accelerating structures, which have been designed when no suitable codes for solving electromagnetic field problems were available. Furthermore, the scheme can help to repurpose available accelerator structures for applications with specifications different from those they were initially designed for.

The method can also be used to examine and optimize the influence of various vacuum to air transitions at the couplers on the beam coupling impedances. In this case, the reference planes for the computation of the generalized scattering matrix are specified so that vacuum-to-air transitions are excluded. Then, the frequency-dependent reflections of the transitions, which contain a window with a matching step, are separately determined and described by the matrices collating the reflections of the structures attached to the vacuum chamber. Finally, the proposed scheme is employed to determine the beam coupling impedances accounting for the various reflections of the vacuum-to-air transitions.

The paper is organized as follows: In Sec. II, the concept of generalized scattering matrices is revised. Thereafter, the approach to determine the beam coupling impedances for arbitrary terminations at the coupler ports of the vacuum chamber is introduced. Section III presents an application of the method. First, a simplified model of the CERN SPS 200 MHz TW structure is used to validate the results from the proposed approach with direct numerical computations using CST Studio Suite® [22]. Then, the scheme is employed to determine an optimal termination impedance for the full TW structure with 33 cells so that the beam coupling impedance is minimized. Finally, Sec. IV provides a summary and conclusions.

II. THEORY

A. Generalized scattering matrices

For the reader's convenience, the basic generalized scattering matrix formalism introduced in [33] is summarized. Extending the conventional scattering matrix by one row and one column to accommodate the beam excitation as an additional port yields

$$\underbrace{\begin{pmatrix} \underline{\mathbf{S}} & \underline{\mathbf{k}} \\ \underline{\mathbf{h}} & \underline{z}_\mathrm{b} \end{pmatrix}}_{\tilde{\underline{\mathbf{S}}}} \underbrace{\begin{pmatrix} \underline{\mathbf{a}} \\ \underline{i}_\mathrm{b} \end{pmatrix}}_{\tilde{\underline{\mathbf{a}}}} = \underbrace{\begin{pmatrix} \underline{\mathbf{b}} \\ \underline{v}_\mathrm{b} \end{pmatrix}}_{\tilde{\underline{\mathbf{b}}}}, \tag{1}$$

where underlined symbols refer to complex-valued quantities that are sampled at a given frequency. The vectors $\underline{\mathbf{a}} \in \mathbb{C}^{N\times 1}$ and $\underline{\mathbf{b}} \in \mathbb{C}^{N\times 1}$ comprise the incident and scattered wave amplitudes corresponding to all N modal excitations at all waveguide boundaries of the structure. The additional entry $\underline{i}_\mathrm{b}$ in the vector $\tilde{\underline{\mathbf{a}}} \in \mathbb{C}^{(N+1)\times 1}$ corresponds to the beam current excitation, $\underline{v}_\mathrm{b}$ in the vector $\tilde{\underline{\mathbf{b}}} \in \mathbb{C}^{(N+1)\times 1}$ to the induced beam voltage, and $\underline{z}_\mathrm{b}$ in the matrix $\tilde{\underline{\mathbf{S}}} \in \mathbb{C}^{(N+1)\times(N+1)}$ to the beam coupling impedance.

B. Beam impedances for arbitrary coupler port terminations

To account for arbitrary termination impedances at the couplers (cf. Fig. 1), the incident and scattered wave amplitudes at the corresponding ports are related by

$$\underline{\mathbf{R}}\,\underline{\mathbf{a}}_\mathrm{ter} = \underline{\mathbf{b}}_\mathrm{ter}, \tag{2}$$

with the block-diagonal matrix

$$\underline{\mathbf{R}} = \mathrm{diag}(\underline{\mathbf{\Gamma}}_{\mathrm{ter},1}, \underline{\mathbf{\Gamma}}_{\mathrm{ter},2}, \ldots, \underline{\mathbf{\Gamma}}_{\mathrm{ter,p}}, \ldots, \underline{\mathbf{\Gamma}}_{\mathrm{ter,P}}). \tag{3}$$

The submatrices $\underline{\mathbf{\Gamma}}_{\mathrm{ter,p}}$ hold the reflection coefficients at the pth waveguide port. In general, multimodal terminations with mode mixing result in fully populated submatrices $\underline{\mathbf{\Gamma}}_{\mathrm{ter,p}}$. In the special case of single-mode scattering at the terminations, these matrices are diagonal matrices and hold the reflection coefficients at the pth waveguide port on their main diagonal:

$$\underline{\mathbf{\Gamma}}_{\mathrm{ter,p}} = \mathrm{diag}(\ldots, \underline{\Gamma}_{m-1}, \underline{\Gamma}_m, \underline{\Gamma}_{m+1}, \ldots). \tag{4}$$

The reflection coefficients $\underline{\Gamma}_m$ of the mth mode are related to the termination impedances $\underline{Z}_{\mathrm{ter},m}$ via

$$\underline{\Gamma}_m = \frac{\underline{Z}_{\mathrm{ter},m} - \underline{Z}_{0,m}}{\underline{Z}_{\mathrm{ter},m} + \underline{Z}_{0,m}}, \tag{5}$$

where $\underline{Z}_{0,m}$ are the port impedances of the mth mode to which the generalized scattering matrix $\tilde{\underline{\mathbf{S}}}$ in (1) is initially

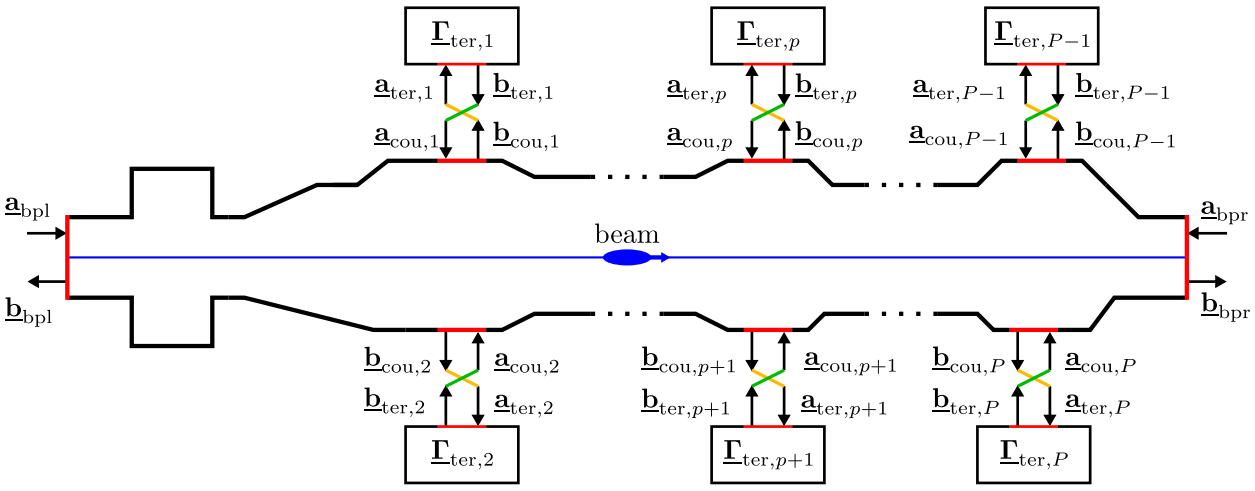

FIG. 1. Schematic representation of an accelerator structure excited by a particle beam with external termination impedances for each mode at each waveguide port. The P waveguide ports are indexed by p. The beam path is marked in blue. The beam enters the structure from the left and leaves the structure on the right. The coupling between various coupler ports and the external termination loads is indicated by green and orange lines, respectively.

normalized to (refer to (2) and (3) in [33]). However, note that single-mode and therefore nonmode mixing terminations are a coarse approximation of the vast majority of real-world setups.

In the next step, the coefficients in the vectors $\underline{\tilde{\mathbf{a}}}$ and $\underline{\tilde{\mathbf{b}}}$ in (1) are reordered using a permutation matrix $\mathbf{P}$:

$$\mathbf{P}\underline{\tilde{\mathbf{a}}} = \begin{pmatrix} \underline{\mathbf{a}}_{\mathrm{cou}} \\ \underline{\mathbf{a}}_{\mathrm{bpl}} \\ \underline{\mathbf{a}}_{\mathrm{bpr}} \\ \underline{i}_{\mathrm{b}} \end{pmatrix}, \qquad \mathbf{P}\underline{\tilde{\mathbf{b}}} = \begin{pmatrix} \underline{\mathbf{b}}_{\mathrm{cou}} \\ \underline{\mathbf{b}}_{\mathrm{bpl}} \\ \underline{\mathbf{b}}_{\mathrm{bpr}} \\ \underline{v}_{\mathrm{b}} \end{pmatrix}. \tag{6}$$

Incident and scattered wave amplitudes with subscripts "bpl" and "bpr" refer to the beam pipe ports at the left and right end of the structure and incident and scattered wave amplitudes with the subscripts "cou" refer to coupler ports. Replacing the vectors $\underline{\tilde{\mathbf{a}}}$ and $\underline{\tilde{\mathbf{b}}}$ in (1) with the reordered vectors defined in (6) and exploiting the orthogonality of the permutation matrix ($\mathbf{P}^{\mathrm{T}} = \mathbf{P}^{-1}$) gives

$$\underbrace{\mathbf{P}\underline{\tilde{\mathbf{S}}}\mathbf{P}^{\mathrm{T}}}_{\underline{\mathbf{G}}} \begin{pmatrix} \underline{\mathbf{a}}_{\mathrm{cou}} \\ \underline{\mathbf{a}}_{\mathrm{bpl}} \\ \underline{\mathbf{a}}_{\mathrm{bpr}} \\ \underline{i}_{\mathrm{b}} \end{pmatrix} = \begin{pmatrix} \underline{\mathbf{b}}_{\mathrm{cou}} \\ \underline{\mathbf{b}}_{\mathrm{bpl}} \\ \underline{\mathbf{b}}_{\mathrm{bpr}} \\ \underline{v}_{\mathrm{b}} \end{pmatrix}. \tag{7}$$

The resulting matrix $\underline{\mathbf{G}}$ is split into blocks according to

$$\underline{\mathbf{G}} = \begin{pmatrix} \underline{\mathbf{G}}_{11} & \underline{\mathbf{G}}_{12} \\ \underline{\mathbf{G}}_{21} & \underline{\mathbf{G}}_{22} \end{pmatrix}, \tag{8}$$

with

$$\begin{aligned} \underline{\mathbf{G}}_{11} &\in \mathbb{C}^{N_{\mathrm{cou}} \times N_{\mathrm{cou}}}, \\ \underline{\mathbf{G}}_{12} &\in \mathbb{C}^{N_{\mathrm{cou}} \times (N_{\mathrm{bpl}} + N_{\mathrm{bpr}} + 1)}, \\ \underline{\mathbf{G}}_{21} &\in \mathbb{C}^{(N_{\mathrm{bpl}} + N_{\mathrm{bpr}} + 1) \times N_{\mathrm{cou}}}, \\ \underline{\mathbf{G}}_{22} &\in \mathbb{C}^{(N_{\mathrm{bpl}} + N_{\mathrm{bpr}} + 1) \times (N_{\mathrm{bpl}} + N_{\mathrm{bpr}} + 1)}. \end{aligned}$$

Here, N_{cou} denotes the total number of waveguide port modes at the couplers, whereas N_{bpl} and N_{bpr} denote the total number of waveguide port modes at the left and the right end of the beam pipe, respectively.

Splitting the system of linear equations (7) using (8) gives

$$\underline{\mathbf{G}}_{11}\underline{\mathbf{a}}_{\mathrm{cou}} + \underline{\mathbf{G}}_{12} \begin{pmatrix} \underline{\mathbf{a}}_{\mathrm{bpl}} \\ \underline{\mathbf{a}}_{\mathrm{bpr}} \\ \underline{i}_{\mathrm{b}} \end{pmatrix} = \underline{\mathbf{b}}_{\mathrm{cou}} \tag{9}$$

and

$$\underline{\mathbf{G}}_{21}\underline{\mathbf{a}}_{\mathrm{cou}} + \underline{\mathbf{G}}_{22} \begin{pmatrix} \underline{\mathbf{a}}_{\mathrm{bpl}} \\ \underline{\mathbf{a}}_{\mathrm{bpr}} \\ \underline{i}_{\mathrm{b}} \end{pmatrix} = \begin{pmatrix} \underline{\mathbf{b}}_{\mathrm{bpl}} \\ \underline{\mathbf{b}}_{\mathrm{bpr}} \\ \underline{v}_{\mathrm{b}} \end{pmatrix}. \tag{10}$$

Connecting the terminations to the coupler ports requires the wave amplitudes scattered from the couplers to match the wave amplitudes incident on the terminations,

$$\underline{\mathbf{b}}_{\mathrm{cou}} = \underline{\mathbf{a}}_{\mathrm{ter}}. \tag{11}$$

Similarly, the wave amplitudes incident on the couplers must equal the wave amplitudes scattered from the terminations,

$$\underline{\mathbf{a}}_{\mathrm{cou}} = \underline{\mathbf{b}}_{\mathrm{ter}}. \tag{12}$$

Multiplying (9) from the left with $\underline{\mathbf{R}}$ and using (2), (11), and (12) gives

$$\underline{\mathbf{R}}\underline{\mathbf{G}}_{11}\underline{\mathbf{a}}_{\mathrm{cou}} + \underline{\mathbf{R}}\underline{\mathbf{G}}_{12} \begin{pmatrix} \underline{\mathbf{a}}_{\mathrm{bpl}} \\ \underline{\mathbf{a}}_{\mathrm{bpr}} \\ \underline{i}_{\mathrm{b}} \end{pmatrix} = \underbrace{\underline{\mathbf{R}}\underline{\mathbf{b}}_{\mathrm{cou}}}_{\underline{\mathbf{a}}_{\mathrm{cou}}}. \tag{13}$$

Solving for the wave amplitudes incident on the couplers results in

$$\underline{\mathbf{a}}_{\mathrm{cou}} = -[\underline{\mathbf{R}}\underline{\mathbf{G}}_{11} - \mathbf{I}]^{-1}\underline{\mathbf{R}}\underline{\mathbf{G}}_{12} \begin{pmatrix} \underline{\mathbf{a}}_{\mathrm{bpl}} \\ \underline{\mathbf{a}}_{\mathrm{bpr}} \\ \underline{i}_{\mathrm{b}} \end{pmatrix}. \tag{14}$$

Finally, replacing (14) in (10) yields

$$\underline{\tilde{\mathbf{S}}}_{\mathrm{mod}} \begin{pmatrix} \underline{\mathbf{a}}_{\mathrm{bpl}} \\ \underline{\mathbf{a}}_{\mathrm{bpr}} \\ \underline{i}_{\mathrm{b}} \end{pmatrix} = \begin{pmatrix} \underline{\mathbf{b}}_{\mathrm{bpl}} \\ \underline{\mathbf{b}}_{\mathrm{bpr}} \\ \underline{v}_{\mathrm{b}} \end{pmatrix}, \tag{15}$$

with the modified generalized scattering matrix

$$\underline{\tilde{\mathbf{S}}}_{\mathrm{mod}} = [\underline{\mathbf{G}}_{22} - \underline{\mathbf{G}}_{21}[\underline{\mathbf{R}}\underline{\mathbf{G}}_{11} - \mathbf{I}]^{-1}\underline{\mathbf{R}}\underline{\mathbf{G}}_{12}] \tag{16}$$

accounting for the termination impedances $\underline{Z}_{\mathrm{ter},m}$ at the coupler ports. In analogy with (1), the right-most entry in the last row of this matrix corresponds to the beam coupling impedance that, now, contains the influence of termination impedances at the coupler ports.

III. NUMERICAL COMPUTATIONS

The TW cavities included in the upgraded baseline of the CERN SPS serve as an application example for the proposed scheme. The SPS acts as the final stage of the Large Hadron Collider (LHC) injector [34,35]. The upgrade of the LHC to the High-Luminosity LHC (HL-LHC) includes an upgrade of the SPS as well. While the SPS TW cavities are operated at

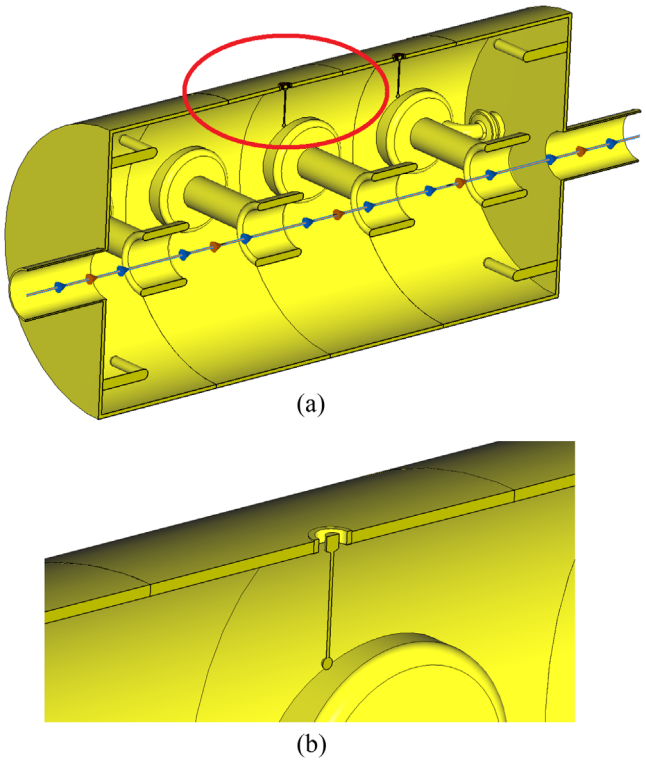

FIG. 2. (a) A simplified, four-cell SPS TW cavity used to compare the proposed scheme with direct computations. (b) Magnification of the red-marked region in (a) showing a probe-type HOM coupler which is terminated with various termination impedances $\underline{Z}_{\mathrm{ter},m}$. The geometry is kindly provided by [37].

200 MHz, the reduction of the beam coupling impedance around 630 MHz is of special relevance to avoid longitudinal multibunch instabilities [30–32]. The conductivity of the cavity walls is assumed to be 5.8×10^7 S/m. The following considerations focus on the real part of the beam coupling impedance, as this quantity determines the instability growth rate (cf. Chapter 4 in [3]).

A. Comparison with direct simulations

To compare the beam coupling impedances obtained by the proposed approach with impedances directly determined by field simulations, the four-cell test arrangement of the SPS TW cavity depicted in Fig. 2 is considered. The four-cell model is not of practical relevance. However, it is chosen such that its longitudinal beam coupling impedance may be conveniently computed by direct simulations with an electromagnetic field solver. In the following simulations, the CST Studio Suite® [22] is employed. The four-cell structure consists of two mirror-symmetric end cells (cf. also Fig. 2(e) in [36]) and two midcells. The midcells are equipped with a so-called probe-type HOM coupler which is depicted in Fig. 2(b) and Fig. 2(b) in [36]. Three different sets of simulations were performed, where the termination impedances $\underline{Z}_{\mathrm{ter}}$ for the TEM mode at both HOM couplers are assumed to be 25 Ω, 32 Ω, and 50 Ω.

The four-cell TW cavity is discretized with CST Studio Suite® using 8,346,240 hexahedral mesh cells. The ends of the HOM couplers are connected to coaxial waveguide ports. The inner conductors of the coaxial lines in the three CST models have the diameters 6.3 mm, 8.5 mm, and 9.6 mm, respectively, whereas the diameters of the outer conductors are 14.5 mm. CST Studio Suite® determines the characteristic impedance of the coaxial waveguide and terminates the port with the respective impedance. This is how the three assumed terminations with 25 Ω, 32 Ω, and 50 Ω at the HOM couplers are implemented in the respective numerical models. The wakefield solver of CST Studio Suite® computes the longitudinal on-axis beam coupling impedances using the finite-integration technique in the time domain [38]. The resulting real parts of the three impedances are depicted in Fig. 3 as dotted lines and serve as reference curves. In addition to the simulations with the wakefield solver of CST Studio Suite®, the beam coupling impedances are determined with the proposed approach. The generalized scattering matrix (1) of the four-cell

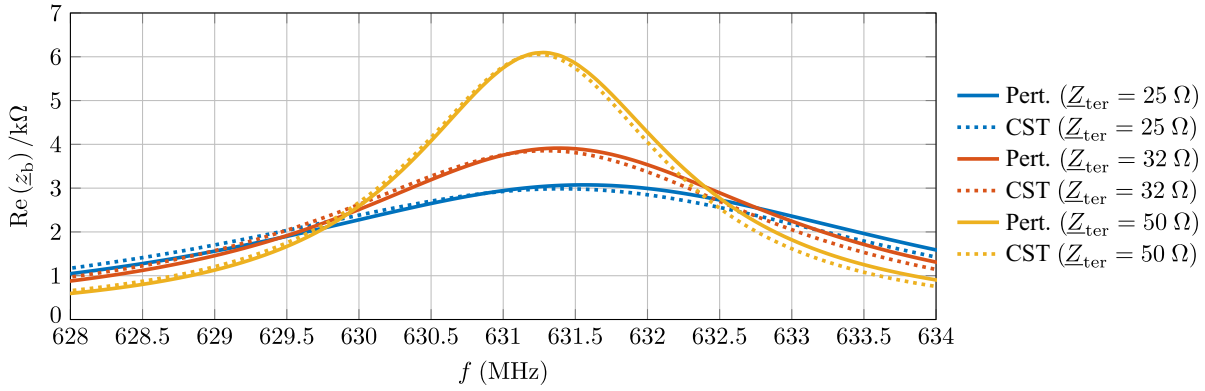

FIG. 3. Real part of the beam coupling impedance of the four-cell SPS TW structure shown in Fig. 2. The blue curves refer to a termination impedance $\underline{Z}_{\mathrm{ter}}$ of 25 Ω, the red curve to 32 Ω, and the orange curve to 50 Ω. The dotted curves are obtained with the wakefield solver of CST studio suite®, whereas the solid curves are obtained by generalized scattering matrix concatenation CSC$^{\mathrm{BEAM}}$ and the approach proposed in this paper for the coupler port terminations.

structure shown in Fig. 2 is calculated with the CSC$^{\text{BEAM}}$ [33] method. In the first step, four generalized scattering matrices for each of the cells are computed using the fourth order–based in-house beam impedance solver described in Sec. II B. in [33]. Each end cell is discretized with 79,299 and each midcell with 97,280 mesh cells. At both beam ports as well as at each decomposition plane between the cells, a large number of waveguide modes consisting of 40 TE- and 40 TM-type modes is considered. The concatenation of the four generalized scattering matrices for each segment delivers the generalized scattering matrix of the four-cell structure shown in Fig. 2. Subsequently, the approach proposed in Sec. II B is applied using the generalized scattering matrix resulting from the concatenation. In close analogy to the direct computation using the CST Studio Suite® code, the termination impedances are chosen to be 25 Ω, 32 Ω, and 50 Ω. The resulting real parts of the three beam coupling impedances for the three termination conditions are depicted in Fig. 3 as solid lines.

Figure 3 shows that the termination impedance at the HOM couplers has a large influence on the real part of the beam coupling impedance. By changing the termination impedance from 50 Ω to 25 Ω, the real part of the beam coupling impedance at the peak can be reduced from 6 kΩ to 3 kΩ. Furthermore, Fig. 3 shows a very good agreement between the dotted and the solid curves. This is quite remarkable given that the dotted curves result from a time-domain approach (including window functions and discrete Fourier transforms) using the finite-integration technique [38] on a hexahedral mesh. In contrast, the solid curves result from a frequency-domain approach using the finite-element method on a hybrid mesh in combination with the concatenation approach [33] and the modified generalized scattering matrix approach for the coupler port terminations (16). Note that the agreement between the imaginary parts of the beam coupling impedances (not shown in the figure) resulting from the two methods is good as well.

B. Application to the SPS TW cavity with 33 cells

We now turn to the investigation of the full 33-cell cavity [30,36]. A direct field simulation of this electromagnetically very large structure is extremely demanding. Thus, a convenient way to consider the influence of termination impedances is the approach presented in this paper. For this sake, generalized scattering matrices of a cell equipped with a loop-type HOM coupler (see Figs. 2(d) and 2(h) in [36]) as well as the corresponding matrix for a cell not equipped with a HOM coupler at all (see Fig. 2(a) in [36]) are additionally computed with the in-house finite-element code. The generalized scattering matrices of the two end cells and the midcell with the probe-type HOM coupler are already available from the validation study with the four-cell model in Sec. III A. In total, the generalized scattering matrices of five different cell types are used. These are concatenated by CSC$^{\text{BEAM}}$ [33] to obtain the beam coupling impedance for the full 33-cell structure. The structure is depicted in Fig. 3(a) in [36] and in Fig. 4(a). Its total length is 12.862 m. Similarly to the computations

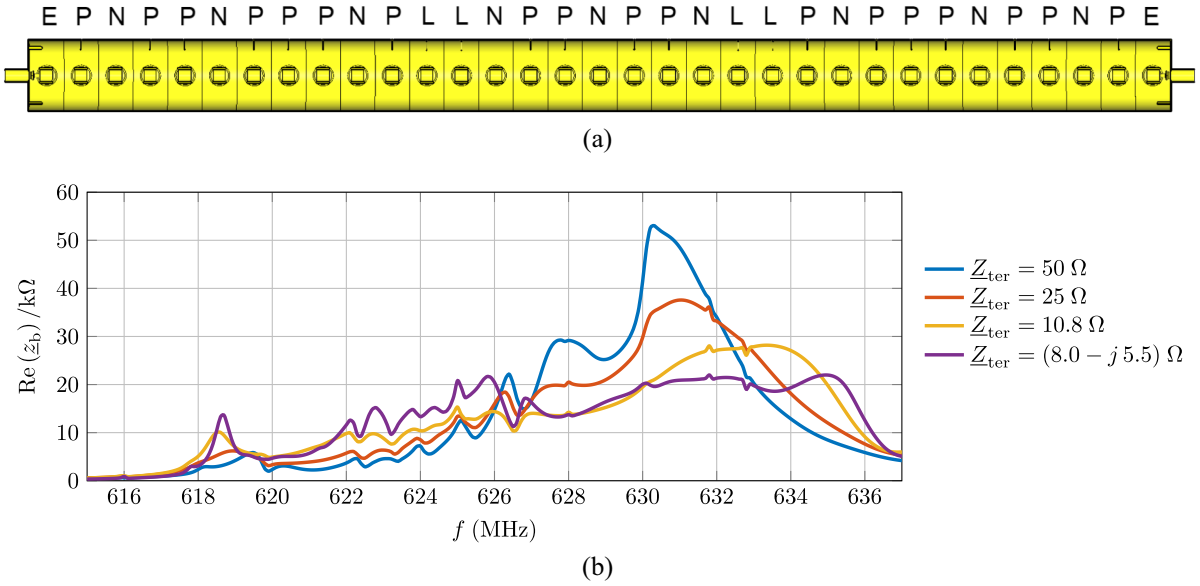

FIG. 4. (a) Cross section of the 33-cell SPS accelerating structure with 18 HOM couplers. The left and the right end cells are marked by an "E," the probe-type couplers by a "P", the loop-type couplers by an "L", and the cells without any couplers by an "N". The geometry is kindly provided by [37] and is plotted with [22]. (b) Real part of the longitudinal beam coupling impedance of the structure shown in (a) for different termination impedances $\underline{Z}_{\text{ter}}$ at each of the 18 HOM couplers.

in Sec. III A, a total of 80 port modes is considered for the concatenation procedure at each of the 32 decomposition planes.

The approach introduced in Sec. II B is used to determine the longitudinal beam coupling impedance for various termination impedances. For simplicity, the same termination impedance $\underline{Z}_{\mathrm{ter}}$ is assumed for all $N_{\mathrm{cou}} = P = 18$ HOM couplers. Note, however, that the method allows to consider an arbitrary combination of termination impedances at the different coupler ports.

Figure 4(b) depicts the real part of the longitudinal beam coupling impedance for different $\underline{Z}_{\mathrm{ter}}$. The blue curve results from the default termination with 50 Ω which is the standard matching impedance on account of 50 Ω systems widely being used in particle accelerator and microwave applications. The red curve arises from a termination of the HOM couplers with 25 Ω. This value is chosen, because it has been already proposed in [30,36] to reduce the real part of the beam coupling impedance at 630 MHz. Note that the red curve in Fig. 4(b) corresponds to the black curve in Fig. 9 in [36]. The orange curve results from terminating the HOM couplers with 10.8 Ω. This value is the optimal, resistive-type impedance $\underline{Z}_{\mathrm{ter}}$ which minimizes the maximal real part of the beam coupling impedance over the depicted frequency range, i.e., the minimization of

$$g = \max_{f_1 \le f \le f_2} \mathrm{Re}(\underline{z}_{\mathrm{b}}), \tag{17}$$

with $f_1 = 615$ MHz, $f_2 = 637$ MHz, and $\mathrm{Re}(\underline{z}_{\mathrm{b}})$ delivering the real part of $\underline{z}_{\mathrm{b}}$. The purple curve is obtained from terminating the HOM couplers with the complex-valued impedance $(8.0 - j5.5)$ Ω. This is the optimal, complex-valued termination impedance $\underline{Z}_{\mathrm{ter}}$ which minimizes g, i.e., the maximal real part of the beam coupling impedance $\underline{z}_{\mathrm{b}}$ over the considered frequency interval. Both optima were obtained in a straightforward manner by sampling the termination impedances on the real axis and in the complex plane with sufficiently small step widths.

Note that there are various ways to realize complex-valued terminations, e.g., by employing impedance transforming networks as discussed in [31]. One simple way to accomplish the complex-valued termination at 631 MHz for the actual example is an ideal lumped resistor with 8 Ω in series with an ideal lumped capacitor having a reactance of $X_C = (2\pi f C)^{-1} = 5.5$ Ω, which results in a capacity of $C = (2\pi f X_C)^{-1} \approx 46$ pF. In fact, this simple RC serial connection is not realistic due to the presence of inductive contributions for nonideal resistors at 631 MHz. For a specific application and depending on the frequency band of interest, these contributions may require further capacitive compensation. The proposed optimal terminations minimize the real part of the beam coupling impedance peak solely at 631 MHz. At other frequencies, the optimal termination might be different. Thus, in general, frequency-dependent terminations are required for broadband beam impedance minimization. Designing such frequency-dependent terminations could be a challenge in itself.

Figure 4 shows again a strong influence of the external impedance loads on the beam coupling impedance. Compared to the 50 Ω termination, a matching circuit with 10.8 Ω leads to a reduction of the real part of the beam impedance by nearly a factor of 2. For a complex termination impedance of $(8.0 - j5.5)$ Ω, the real part of the beam coupling impedance is even more reduced by a factor of 2.5. Thus, a considerable improvement in the cavity operation and higher beam stability thresholds can be achieved with little effort by proper modification of the impedance loads at the coupler ports.

IV. SUMMARY AND CONCLUSIONS

An efficient method to compute beam coupling impedances as a function of termination impedances of the matching circuits at the coupler ports is introduced. The method is based on the generalized scattering matrix approach. This matrix has to be numerically computed only once with given port terminations. Then, the scheme readily enables the computation of beam coupling impedances for arbitrary port terminations. Thus, the method allows for systematically studying the influence of the matching circuits on beam coupling impedances without the computational burden required for these studies using direct field simulations. Moreover, the influence of various vacuum-to-air transitions at the couplers on the beam coupling impedances can be readily determined. This paper provides a numerical comparison study for a simplified four-cell TW cavity model demonstrating the validity of this approach. The application of the scheme for a full 33-cell 200 MHz TW structure of the SPS shows that coupling impedances can be substantially reduced in the critical frequency range. Particularly, for already existing cavity structures, modifying port termination impedances is a feasible way to reduce beam-coupling impedances without the need to redesign the coupler system. The proposed scheme allows for designing suitable matching circuits that minimize the influence of the wakefields on the particle beam.

ACKNOWLEDGMENTS

The authors would like to thank Kai Papke for fruitful discussions on the design of HOM couplers and for reviewing the manuscript prior to its submission.

[1] T. Weiland and R. Wanzenberg, Wake fields and impedances, *Frontiers of Particle Beams: Intensity Limitations: Proceedings of a Topical Course held by the Joint US-CERN School on Particle Accelerators, Hilton Head Island, South Carolina, 7-14 November 1990*, Lecture

Notes in Physics Vol. 400 (Springer, Berlin, Heidelberg, 1992), p. 39.
[2] L. Palumbo, V. Vaccaro, and M. Zobov, Wake fields and impedance, Report No. LNF-94-041-P, (1994), p. 331.
[3] A. W. Chao, *Physics of Collective Beam Instabilities in High Energy Accelerators*, Wiley Series in Beam Physics and Accelerator Technology (Wiley, New York, 1993).
[4] V. G. Vaccaro, Longitudinal instability of a coasting beam above transition, due to the action of lumped discontinuities, CERN, Geneva, Switzerland, CERN Report No. ISR-RF/66-35, 1966.
[5] V. G. Vaccaro, The birth and childhood of a couple of twin brothers, in *Proceedings of ICFA Mini-Workshop on Impedances and Beam Instabilities in Particle Accelerators, Benevento, Italy* (CERN,Geneva, 2017), pp. 117–123.
[6] A. Lasheen, T. Argyropoulos, T. Bohl, J. F. Esteban Müller, H. Timko, and E. Shaposhnikova, Beam measurement of the high frequency impedance sources with long bunches in the CERN Super Proton Synchrotron, Phys.Rev. Accel. Beams **21**, 034401 (2018).
[7] J. Liu, J. C. Yang, J. W. Xia, D. Y. Yin, G. D. Shen, P. Li, B. Wu, S. Ruan, H. Zhao, G. Wang, Z. Q. Dong, K. D. Wang, and L. P. Yao, Transverse impedances and collective instabilities in a heavy ion accelerator, Phys. Rev. Accel. Beams **21**, 064403 (2018).
[8] E. Métral *et al.*, Beam instabilities in hadron synchrotrons, IEEE Trans. Nucl. Sci. **63**, 1001 (2016).
[9] U. Niedermayer, L. Eidam, and O. Boine-Frankenheim, Analytic modeling, simulation and interpretation of broadband beam coupling impedance bench measurements, Nucl. Instrum. Methods Phys. Res., Sect. A **776**, 129 (2015).
[10] H.-W. Glock, M. Abo-Bakr, J. Kolbe, F. Pflocksch, C. Potratz, and A. Schälicke, Loss factor and impedance analysis of warm components of BERLinPro, in *Proceedings of the 6th International Particle Accelerator Conference, IPAC-2015, Richmond, VA, 2015* (JACoW, Geneva, Switzerland, 2015), pp. 128–131.
[11] U. Niedermayer and O. Boine-Frankenheim, Analytical and numerical calculations of resistive wall impedances for thin beam pipe structures at low frequencies, Nucl. Instrum. Methods Phys. Res., Sect. A **687**, 51 (2012).
[12] U. Niedermayer, Determination of beam coupling impedance in the frequency domain, Ph.D. thesis, Technische Universtät Darmstadt, 2015.
[13] U. Niedermayer, O. Boine-Frankenheim, and H. De Gersem, Space charge and resistive wall impedance computation in the frequency domain using the finite element method, Phys. Rev. ST Accel. Beams **18**, 032001 (2015).
[14] S. A. Heifets and S. A. Kheifets, Coupling impedance in modern accelerators, Rev. Mod. Phys. **63**, 631 (1991).
[15] A. V. Smirnov and J. Zeng, Analytical characterization of fundamental mode in pillbox cavities with beam pipe, Nucl. Instrum. Methods Phys. Res., Sect. A **452**, 44 (2000).
[16] A. Al-Khateeb, O. Boine-Frankenheim, A. Plotnikov, S. Shim, and L. Hänichen, Longitudinal impedance of a step-in for a round beam at arbitrary beam energy, Nucl. Instrum. Methods Phys. Res., Sect. A **626–627**, 1 (2011).
[17] M. R. Masullo, S. Petracca, and G. Rumolo, A general overview on the 2017 ICFA Mini-Workshop on impedances and beam instabilities in particle accelerators, in *Proceedings of ICFA Mini-Workshop on Impedances and Beam Instabilities in Particle Accelerators, Benevento, Italy* (CERN, Geneva, 2017) pp. 1–4.
[18] I. Zagorodnov and T. Weiland, TE/TM field solver for particle beam simulations without numerical Cherenkov radiation, Phys. Rev. ST Accel. Beams **8**, 042001 (2005).
[19] E. Gjonaj, T. Lau, T. Weiland, and R. Wanzenberg, Computation of short range wake fields with PBCI, ICFA Beam Dyn. Newsletter, **45**, 38 (2008).
[20] W. Bruns, GdfidL: A finite difference program with reduced memory and cpu usage, in *Proceedings of the Particle Accelerator Conference, Vancouver, BC, Canada* (IEEE, New York, 1997), Vol. 2, pp. 2651–2653.
[21] *Advanced Computational Electromagnetics 3P*, SLAC National Accelerator Laboratory, Menlo Park, CA.
[22] CST Studio Suite 2021 (Dassault Systemes Deutschland GmbH, Meitnerstr. 8, 70563 Stuttgart, Germany).
[23] R. E. Collin, *Foundations for Microwave Engineering* (McGraw-Hill Ryerson, Limited, New York, 1992).
[24] L. Nickelson, *Electromagnetic Theory and Plasmonics for Engineers* (Springer, Singapore, 2019).
[25] E. Haebel, Couplers, tutorial and update, in *Proceedings of the Fifth Workshop on RF Superconductivity, Hamburg, Germany* (1991), pp. 334–353, https://accelconf.web.cern.ch/SRF91/papers/srf91d05.pdf.
[26] E. Haebel, Couplers for cavities, in *Proceedings of Superconductivity in Particle Accelerators, CERN Accelerator School, Hamburg, Germany* (1996) pp. 231–231, https://cds.cern.ch/record/308016/files/p231.pdf.
[27] F. Gerigk, Design of higher-order mode dampers for the 400 MHz LHC superconducting cavities, Studienarbeit Technische Universität Berlin, 1997, 10.13140/RG.2.2.36395.64802.
[28] H. Padamsee, T. Hays, and J. Knobloch, *RF Superconductivity for Accelerators*, Wiley Series in Beam Physics and Accelerator Technology (Wiley, New York, NY, 1998).
[29] K. Papke, F. Gerigk, and U. van Rienen, Comparison of coaxial higher order mode couplers for the CERN Superconducting Proton Linac Study, Phys. Rev. Accel. Beams **20**, 060401 (2017).
[30] P. Krämer and C. Völlinger, HOM-Mitigation for future SPS 33-Cell 200 MHz accelerating structures, in *Proceedings of the 13th International Computational Accelerator Physics Conference, Key West, FL* (JACoW, Geneva, Switzerland, 2018), pp. 35–41.
[31] P. Krämer, Studies of higher order mode couplers for the upgraded travelling wave acceleration system in the CERN SPS, Ph.D. thesis, RWTH Aachen, 2020.
[32] J. Repond, Possible mitigations of longitudinal intensity limitations for HL-LHC beam in the CERN SPS, Ph.D. thesis, École Polytechnique Fédérale de Lausanne, 2019.
[33] T. Flisgen, E. Gjonaj, H.-W. Glock, and A. Tsakanian, Generalization of coupled S-parameter calculation to compute beam impedances in particle accelerators, Phys. Rev. Accel. Beams **23**, 034601 (2020).
[34] J. Coupar *et al.*, LHC injectors upgrade, technical design report, Report No. CERN-ACC-2014-0337, 2014, https://cds.cern.ch/record/1976692?ln=de.

[35] O. Aberle *et al.*, High-luminosity large hadron collider (HL-LHC): Technical design report, Report No. CERN-2020-010, https://cds.cern.ch/record/2749422?ln=de.

[36] S. G. Zadeh, E. Gjonaj, T. Flisgen, P. Krämer, C. Völlinger, and U. van Rienen, Impedance minimization of the SPS cavities using the generalized coupled S-parameter method, Phys. Rev. Accel. Beams **25**, 082001 (2022).

[37] P. Krämer (private communication).

[38] T. Weiland, Eine Methode zur Lösung der Maxwellschen Gleichungen für sechskomponentige Felder auf diskreter Basis, Archiv der elektrischen Übertragung **31**, 116 (1977).